TWO ELEMENTARY MODELS FOR THE REGULATION OF SKELETAL MUSCLE CONTRACTION BY CALCIUM

TERRELL L. HILL
Laboratory of Molecular Biology, National Institute of Arthritis, Diabetes, and Digestive and Kidney Diseases, National Institutes of Health, Bethesda, Maryland 20205 and Department of Pharmacology, Biozentrum, University of Basel, 4056 Basel, Switzerland

ABSTRACT   It is shown by use of an extremely simple explicit two-state model that two basic ideas may be sufficient to understand at least qualitatively the sensitive activation of isometric muscle contraction by Ca^{2+}. (a) Ca^{2+} binds much more strongly on troponin if myosin is already attached to actin. The steady state analogue of this is that the single rate constant (in the two-state model) for myosin attachment plus P_i release is much larger if Ca^{2+} is bound to troponin. (b) End-to-end tropomyosin interactions are responsible for positive cooperativity. Although these ideas seem to be sufficient, this of course does not mean that they are necessary. These same ingredients were used in two previous, more elaborate models for the cooperative equilibrium binding of myosin subfragment-1 on actin-tropomyosin-troponin, with and without Ca^{2+}, and for a study of the steady state ATPase activity of the same system. Essentially as an appendix, the above-mentioned simple treatment is extended to a somewhat more realistic and complicated model of isometric contraction.

INTRODUCTION

A general outline of the roles of calcium and cooperativity in the regulation of skeletal muscle has been available for some time (1–6). Also, a general theoretical formalism exists (7–13) that interconnects the structure, biochemistry, and biophysics of activated skeletal muscle. The purpose of this paper is to present two of the most elementary examples possible that extend the theoretical formalism to include the regulation problem for steady isometric contractions. These models are so simple, in fact, essentially pedagogical, that the quantitative results obtained should not be taken very seriously. However, these examples appear to contain at least one possible set of sufficient ingredients for the combined problem. They should therefore be quite helpful in the future in extending the treatment to models that are much more realistic in various ways. A more elaborate analysis would be extremely model dependent (details of structure, of regulation mechanism, and of biochemical mechanism). It therefore seems a little premature to attempt such a calculation at the present time. The complexities of the full problem will surely require a Monte Carlo computational approach if mathematical approximations are to be avoided. The present models are of value primarily because they provide an opportunity to view the elements of the problem in simple analytical form.

The cooperativity in S-1 (subfragment-1 of heavy meromyosin) binding to regulated actin (i.e., actin saturated with tropomyosin-troponin) (14) is presumably due to interactions between the ends of neighboring tropomyosin molecules (15). We have used this feature in several previous theoretical papers (16–19) on cooperative equilibrium and steady state S-1 activity, employing two different models. In the present work, our second model (18, 19) of tropomyosin response to Ca^{2+} and myosin is adopted, but only because it is simpler. The other model (16, 17) may well prove to fit the relevant experiments better.

To simplify the biochemistry as much as possible, we adopt a two-state ATPase cycle, with one attached state and one unattached state. Such a cycle, of course, omits too many biochemical details (6, 13) but it does suffice to provide a semiquantitative understanding of much of muscle biophysics (7, 12). One unfortunate complication inherent in the use of a two-state cycle is the fact that the "attachment" step includes both attachment and P_i release. Reference 6 should be consulted to compare the full kinetic diagram with the two-state cycle used here.

As to structure, in the so-called overlap region between thick and thin filaments there is one actin monomer per $55/2$ Å in a thin filament, and there is one myosin molecule, or cross-bridge (two heads), per $143/3$ Å (20, 21) in a thick filament. Because there are twice as many thin as thick filaments, the number of cross-bridges per seven actin monomers (the number covered by one tropomyosin molecule) in the overlap region is then 2.02. For maximum simplicity, again, we therefore assume (a) that there are exactly two cross-bridges per Tm (tropomyosin) unit, presumably not from the same thick filament, (b) that only one particular thin filament site (out of seven) is suitably oriented for attachment of each cross-bridge (Fig.

1 *A*), and (*c*) that only one of the two heads of a cross-bridge can attach to actin at a time. Previous calculations (12, 13, 22) indicate that the single-site assumption, *b* above, leads to a calculated mechanical force too small by a factor of ~2 (the same is found in the present work). Presumably, then, the assumed one-site specificity is too strong and, instead, two or three neighboring actin sites should be made available, in models, per cross-bridge. However, this complicates the kinetic diagram considerably (10, 22), so we omit this refinement.

An important feature included in the theoretical formalism mentioned above (9, 11) is the uniform averaging (*z* averaging, below) over relative myosin-actin site positions. With the simplifying assumption, *a* above, of an integral number of cross-bridges per Tm unit (seven actin sites), this uniform averaging (to avoid periodic properties not observed) would have to have its origin in the random phases (myosin-actin site distances) of different fibrils in a single muscle fiber or of different filaments in a single fibril, or both. The integral assumption is used for a technical reason: it makes each unit in the one-dimensional array of Tm units (Fig. 1 *A*) equivalent, and hence leads to cooperativity calculations that are much simpler than they would otherwise be. Incidentally, each thin filament has a length of ~1 μm, so that there are ~26 Tm units per thin filament. The cooperativity calculations given in these two papers will ignore end effects (i.e., the calculations apply strictly to an infinite filament). A finite filament can be used in future Monte Carlo calculations (along with numerous other refinements); in fact, a finite filament is an advantage for Monte Carlo calculations.

Fig. 2 illustrates the properties we assume for Tm-Tn (Tn, troponin), when Ca^{2+} or S-1, or both, are bound or attached. The properties are the following (19). Tm-Tn blocks the binding sites on the thin filament. When Ca^{2+} is bound, but not S-1, there is a conformational change in Tn that moves Tm relative to the actin sites. This movement of Tm requires expenditure of free energy, which would be reflected in the binding constants of Ca^{2+}. Tm is moved even further, with a greater cost in free energy, when the first S-1 is bound or attached to a site of the unit, in the absence of Ca^{2+}. If the unit is already saturated with Ca^{2+},
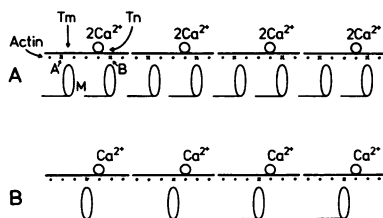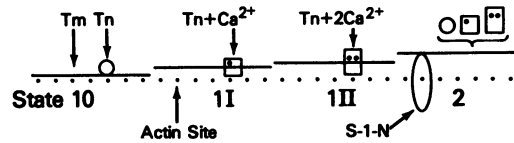
FIGURE 2 Schematic representation of four states of tropomyosin-troponin used in binding model (19). Troponin undergoes a conformational change (circle, square, rectangle) when Ca^{2+} is bound (heavy point), causing tropomyosin-troponin (*Tm-Tn*) to change position in relation to the actin sites when tropomyosin-troponin is in state 1 (substates 10, 1I, 1II, according to number of Ca^{2+} bound). When *S-1-N* (*N*, nucleotide) is bound, tropomyosin-troponin is in state *2*, with a position relative to actin sites that is independent of troponin conformation.

attachment of the first S-1 requires less work against Tm: the attachment or binding constant of S-1 is correspondingly larger. Once one S-1 is attached to a unit, binding of either Ca^{2+} or additional S-1 requires no further work against Tm: these binding or attachment constants, for Ca^{2+} or S-1, are therefore maximal.

As will be seen below, there are two essential ingredients in the regulation part of the problem, for the model adopted here. (*a*) Ca^{2+} binds more strongly to Tn if S-1 is already attached to actin (1) or, equivalently, either at equilibrium (1) or at steady state (23), S-1 attaches more strongly to actin if Ca^{2+} is already bound to Tn. This steady-state effect is a consequence of an increase in the rate constant for the step that includes P_i release (23). (*b*) There is strong positive cooperativity in the system (14, 15) owing to nearest-neighbor Tm-Tm interactions. The latter property sharpens the response to the former.

Sections 1–3 treat an even simpler system than that outlined above (Figs. 1 *A* and 2), namely, the hypothetical model shown in Fig. 1 *B* in which there is only one cross-bridge per Tm unit and only one Ca^{2+} binding site per Tn. Even this elementary system retains the essential Ca^{2+} and cooperativity features of skeletal muscle regulation. In sections 4 to 6 this treatment is extended to the somewhat more realistic and complicated model in Figs. 1 *A* and 2. Even this modest refinement leads to considerable new complexity.

We start in section 1 (and again in section 4) with the equilibrium attachment problem. This is done not because it is thought that regulation is essentially an equilibrium problem but rather, again, for a technical reason: If a two-state cycle is used to handle the steady state problem, then it is possible to cast the steady state analysis into quasi-equilibrium form. Hence, relatively simple equilibrium results can be taken over, for the steady state, without formal change. This cannot be done if three or more states are used in the kinetic cycle. In this latter case the theoretical problem is much more formidable. Despite the equilibrium flavor at the outset, regulation proves here to be a kinetic, not an equilibrium, problem (cf. Chalovich and Eisenberg [23]).

FIGURE 1 (A) Model for binding two Ca^{2+} on troponin (*Tn*) and two myosin (*M*) on specific actin sites *x*(*A* and *B*). Tm is tropomyosin. (*B*) Simpler model used in sections 1–3 with one Ca^{2+}, one *M*, and one specific actin site *x* per Tm unit.

1. EQUILIBRIUM ATTACHMENT OF MYOSIN, MODEL 1

We consider first an equilibrium version of the model and then turn to the steady state case. This procedure is useful because the steady state treatment has a close formal resemblance to the equilibrium treatment. The system of interest is the one-dimensional lattice of units in Fig. 1 B, with nearest-neighbor Tm-Tm interactions. An isolated individual unit (no neighbor interactions) can exist in four different states (a, b, c, d), as shown in Fig. 3. The analogue of Fig. 2 for the present simpler model is presented in Fig. 4. When Ca^{2+} is not bound to Tn (Fig. 3), the attachment equilibrium constant of M (myosin cross-bridge) to A (the specific actin site, x) is K. This is a dimensionless constant (M is part of the myofilament structure and does not have a concentration) for the process $a \to b$. Included in K (i.e., reducing its value) is the work necessary to move Tm (Fig. 4). When M is not attached to A (Fig. 3), the binding constant of Ca^{2+} to Tn is K_a (process $a \to c$). The concentration of Ca^{2+} is ρ. When M is attached to A, the binding constant of Ca^{2+} to Tn is K_b (process $b \to d$). It is much easier to bind Ca^{2+} when M is attached (Fig. 4): $K_b \gg K_a$. We shall use the ratio $K_b/K_a = 20$, as an example. This is based on the value of the corresponding ratio (19) in sections 4–6, evaluated from data in reference 1.

The grand partition function (24) for an isolated unit is then

$$\xi = 1 + K + K_a\rho + K_b\rho \cdot K, \tag{1}$$

where the individual terms are proportional to the populations of the corresponding states (Fig. 3) at equilibrium. Thus, because $K_b \gg K_a$, M attaches to A much more readily when Ca^{2+} is bound to Tn (see also Fig. 4): when Ca^{2+} is not bound, the attachment constant of M is K; when Ca^{2+} is bound, the attachment constant of M is $(K_b/K_a)K$ (Fig. 3).

At an arbitrary ρ, the probability θ that M is attached, in an isolated unit, follows from Eq. 1:

$$\theta = K(1 + K_b\rho)/\xi. \tag{2}$$

The two limiting cases of interest are

$$\theta = K/(1 + K) \qquad (\rho = 0) \tag{3}$$

$$= (K_b/K_a)K/[1 + (K_b/K_a)K]. \qquad (\rho = \infty) \tag{4}$$

For example, if $K = 0.2$ and $K_b/K_a = 20$, then $\theta = 0.167$ when $\rho = 0$, and $\theta = 0.8$ when $\rho = \infty$.

We now consider a one-dimensional array (Fig. 1 B) of these units, at equilibrium. At this point, Tm-Tm interactions have to be introduced explicitly. These are responsible for the cooperativity in the system. Fig. 4 is pertinent here. In this figure, the states are classified and relabeled (0, 1, 2) according to the position of Tm relative to the actin sites. As in reference 19, we assume an optimal
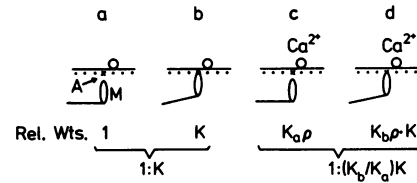

FIGURE 3 Four states of an isolated unit taken from Fig. 1 B, at equilibrium. The relative weights (Rel. Wts.) of the four states are given by grand partition function terms.

Tm-Tm interaction if two neighboring units are in the same position or state (0, 1, or 2) and less favorable interactions the larger the position difference of two neighbors. This assumption is consistent with the equilibrium S-1 binding data (19). If we let w_{ij} be the interaction free energy (a negative quantity, relative to infinite separation) between two Tm neighbors in states i and j (or j and i), and define $x_{ij} = e^{-w_{ij}/kT}$, then we take (in accordance with the above discussion)

$$x_{00} = x_{11} = x_{22} \equiv x, \qquad x > x_{01}, x_{12} > x_{02}. \tag{5}$$

The exact equilibrium properties of the one-dimensional array can be deduced using the well-known matrix method (25). Because of the three states 0,1,2, we need a 3×3 matrix here. The single-unit grand partition function terms, namely, $1, K_a\rho$, and $K(1 + K_b\rho)$, for states $k = 0,1,2$ are entered in the successive rows of the matrix. These entries refer to the kth unit in the linear array. The columns relate to the $k + 1$th unit, which may also be in any one of the states 0,1,2. The appropriate Boltzmann factor for the $k, k + 1$ neighbor interaction is then multiplied into each matrix element. Thus the complete 3×3 matrix in this case is

$$\begin{pmatrix} x & x_{01} & x_{02} \\ K_a\rho x_{01} & K_a\rho x & K_a\rho x_{12} \\ K(1 + K_b\rho)x_{02} & K(1 + K_b\rho)x_{12} & K(1 + K_b\rho)x \end{pmatrix}. \tag{6}$$

If γ_{max} is the largest eigenvalue of this matrix, then the grand partition function for a long array of m units is $\Xi = \gamma_{max}^m$. Because there is a factor K in the matrix for each attached M (myosin), the equilibrium fraction of units with M attached is given by

$$\theta = K\partial\ln\gamma_{max}/\partial K. \tag{7}$$

This can be evaluated numerically for arbitrary ρ.

In the limiting case $\rho \to 0$ (no Ca^{2+}), the matrix
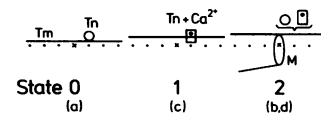

FIGURE 4 Simpler version of Fig. 2 for the model used in sections 1–3. The state labels a, b, c, d are from Fig. 3.

simplifies to (states a and b, Fig. 3)

$$\begin{pmatrix} x & x_{02} \\ Kx_{02} & Kx \end{pmatrix}. \tag{8}$$

Here we find (26)

$$\theta = 2KY_0^{-1}/R_0(1 - K + R_0) \tag{9}$$

$$R_0 = [(1 - K)^2 + 4KY_0^{-1}]^{1/2}$$

$$Y_0 = x^2/x_{02}^2 > 1,$$

where Y_0 is the effective cooperativity parameter in the absence of Ca^{2+}. $Y_0 > 1$ (see Eq. 5) corresponds to positive cooperativity. We shall take $Y_0 = 20$ (19) as typical. Y_0 is larger the larger the incompatibility between two Tm ends in states 0 and 2 (Fig. 4) relative to two Tm ends in states 0,0 or 2,2. Y_0 depends on the nucleotide bound to M (19).

In the limiting case $\rho \rightarrow \infty$ (Tn saturated with Ca^{2+}), the matrix is (states c and d, Fig. 3)

$$\begin{pmatrix} K_a\rho x & K_a\rho x_{12} \\ KK_b\rho x_{12} & KK_b\rho x \end{pmatrix}. \tag{10}$$

From this we obtain (26)

$$\theta = 2(K_b/K_a)KY_\infty^{-1}/R_\infty[1 - (K_b/K_a)K + R_\infty] \tag{11}$$

$$R_\infty = \{[1 - (K_b/K_a)K]^2 + 4(K_b/K_a)KY_\infty^{-1}\}^{1/2}$$

$$Y_\infty = x^2/x_{12}^2 > 1.$$

Note that Eq. 11 has the same functional form as Eq. 9, but $(K_b/K_a)K$ replaces K, and Y_∞ replaces Y_0. Although $Y_\infty > 1$ (positive cooperativity), $Y_\infty < Y_0$ (Eq. 5). We take $Y_\infty = 4$ (16) as a representative value.

If each element in Eq. 6 is divided by x, we see that in this more general case (arbitrary ρ), a third effective interaction parameter appears: $Y_1 \equiv x^2/x_{01}^2 > 1$ (Eq. 5). A simple energetic argument in relation to Fig. 4 suggests that $Y_1 = Y_0/Y_\infty$, so we take $Y_1 = 5$, below, as typical.

The right-hand curve in Fig. 5 is a plot of θ (fraction of M attached) against log K, using Eq. 9 (i.e., in the absence of Ca^{2+}) with $Y_0 = 20$. On this curve, $\theta = \frac{1}{2}$ at $K = 1$ (Eq. 9). The left-hand curve in Fig. 5 shows θ as a function of log K, as calculated from Eq. 11 (i.e., with Ca^{2+} saturation), using $K_b/K_a = 20$ and $Y_\infty = 4$. This latter curve has $\theta = \frac{1}{2}$ at $K_bK/K_a = 1$, that is, at $K = 0.05$.

The two curves in Fig. 5 contain an equilibrium version of muscle regulation by Ca^{2+}. If the attachment equilibrium constant for M, in the absence of Ca^{2+}, has a value significantly <1, e.g., $K = 0.2$, while the attachment constant for M in the presence of Ca^{2+} has a value significantly >1, e.g., $(K_b/K_a)K = 4$, then the introduction of Ca^{2+} into the system can result in a dramatic increase in the probability θ of attachment of M. This is illustrated by the long vertical arrow in Fig. 5 placed at $K = 0.2$ along the abscissa. Here θ increases from 0.015 to 0.916 when Ca^{2+}
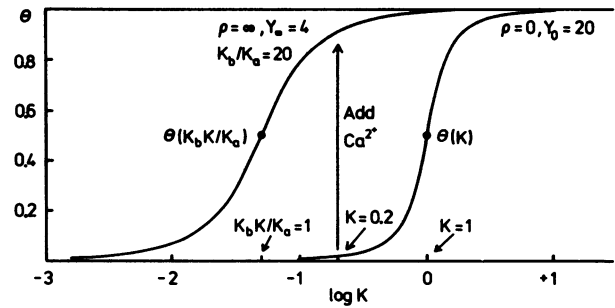

FIGURE 5 Plots of θ from Eqs. 9 and 11 as functions of log K. These curves correspond to extreme Ca^{2+} concentrations ($\rho = 0$, $\rho = \infty$). The vertical arrow shows the change in θ when Ca^{2+} is added, if $K = 0.2$.

is added. Cooperativity plays a significant role in this result. In the absence of cooperativity ($Y_0 = Y_\infty = 1$), as already considered following Eq. 4, the corresponding increase in θ would be less impressive: $\theta = 0.167$ to 0.8. Note also that there would be significant attachment ($\theta = 0.167$) in the absence of Ca^{2+}. Fig. 5 is analogous to Fig. 2 in reference 16, where K_2c corresponds to K here.

The above effect of Ca^{2+} addition is shown in more detail in Fig. 6, where the solid curve is θ as a function of log $K_a\rho$ along the vertical arrow in Fig. 5 (only the end points are given in Fig. 5). This curve (Fig. 6) has been calculated numerically from Eq. 7, using $Y_1 = 5$ as well as the other parameters already mentioned. The analogue in reference 16 is the dashed curve in Fig. 3.

Because a cross-bridge cannot exert force on an actin filament unless it is attached (9, 11), the result in Fig. 6 for the equilibrium degree of attachment is what is needed qualitatively. Of course, at steady state, attachment is governed by rate constants (see below), not equilibrium constants. Isometric force is activated when the Ca^{2+} concentration ρ is increased by a factor of ~100 (from 10^{-7} M to 10^{-5} M). This corresponds to 2 units on the abscissa of Fig. 6. The degree of cooperativity in this figure, that is, the sharpness in the rise in θ, is seen to be consistent with this observation. It should be emphasized that the values of
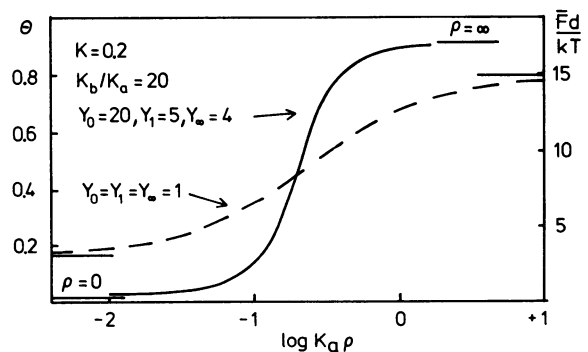

FIGURE 6 Change in θ as a function of log ρ (Ca^{2+}) along the vertical arrow in Fig. 5 (i.e., with $K = 0.2$), as calculated from Eqs. 6 and 7. The broken curve is obtained in the absence of cooperativity. In the example leading to Eq. 31, θ is proportional to the isometric force $\bar{F}$ (right ordinate).

the cooperativity parameters being used here are based on equilibrium S-1 · ADP binding data (16, 19). Larger parameter values would lead to sharper curves. Indeed, the values of Y_o, Y_1, and Y_∞ are expected to depend (19) on the conformation of the attached myosin and on the bound nucleotide in the attached state.

The broken curve in Fig. 6 is what is found in the absence of cooperativity ($Y_o = Y_1 = Y_\infty = 1$). This curve has been calculated from Eq. 2, using $K = 0.2$ and $K_b/K_a = 20$. We turn now to the corresponding steady state problem.

2. THE STEADY STATE (ISOMETRIC) SYSTEM, MODEL 1

To maintain our policy of maximum simplicity, we adopt a two-state cycle, shown in Fig. 7 A, to represent the ATPase activity of M, as well as attachment-detachment of M to actin (6, 13). The schematic diagrams in Figs. 1 B, 3, and 4 are still applicable, but attachment is now part of a two-state cycle and, in fact, can be achieved in principle by two different biochemical routes, shown in Fig. 7 A (release of P_i; and release of T, binding of D). Note that neither route involves just simple attachment; in both cases other elementary events are included. Fig. 7 B and C, shows, with simpler notation, the same two-state cycle, without and with Ca^{2+} bound to Tn, and the first-order rate constants that we adopt for these cycles for a single, isolated Tm unit. These rate constants are perturbed by neighbor interactions in the array in Fig. 1 B, as discussed below. Fig. 8 A and B, presents the corresponding free energy curves (12). In one complete cycle (either α, β, or κ, λ), the free energy of Tm + Tn + M drops by an amount $\Delta\mu_{ATP} \equiv \Delta kT$, the free energy of hydrolysis of ATP ($\sim$13 kcal mol^{-1}).

The free energy of the attached state is a function of z, a variable (usually called x) that locates the axial position of M relative to its specific actin site. We take this function to be a parabola (again, the simplest choice). $K_\alpha(z)$ is the attachment constant of M at z in Fig. 8 A (no Ca^{2+}) via the α, α' transitions and $K_\beta(z)$ is the (very weak) attachment constant via β', β. The corresponding (larger) attachment constants in Fig. 8 B (Ca^{2+} bound) are $K_b K_\alpha(z)/K_a$ via the κ, κ' transitions and $K_b K_\beta(z)/K_a$ via λ', λ. $K_\alpha(z)$ and $K_\beta(z)$

are both analogues of K in Fig. 3. K_a is independent of z because it refers to binding of Ca^{2+} on Tn with M unattached (hence z cannot be involved). We take K_b to be a constant as well, though in principle it could be a function of z (e.g., if the angle of attachment of S-1 to actin varies with z). With K_a and K_b chosen as constants, the two parabolas in Fig. 8 are the same except for vertical displacement; the left one (no Ca^{2+}) is higher by an amount $kT\ln(K_b/K_a)$. The deeper free energy well in Fig. 8 B corresponds to tighter attachment of M to A when Ca^{2+} is bound.

The eight rate constants in Fig. 8 are also, in general, all functions of z. We assume that Ca^{2+} binding and release are relatively fast processes, always at equilibrium. Hence corresponding rate constants need not be introduced.

If the lowest free energy level in either Fig. 8 A or 8 B is chosen as zero, then the top (constant) level is ΔkT and the attached state has free energy:

$$\text{no } Ca^{2+} \quad kT[\Delta - \Gamma_o + (z^2/2\sigma^2)]$$
$$= kT[\Delta - \ln K_\alpha(z)] \quad (12)$$

$$Ca^{2+} \quad kT[\Delta - \Gamma_\infty + (z^2/2\sigma^2)]$$
$$= kT[\Delta - \ln(K_b K_\alpha(z)/K_a), \quad (13)$$

where kT/σ^2 is the force constant of the free energy curve. Other useful relations (12) are

$$\alpha(z)/\alpha'(z) = K_\alpha(z) = \exp[\Gamma_o - (z^2/2\sigma^2)] \quad (14)$$

$$\beta(z)/\beta'(z) = 1/K_\beta(z) = \exp[\Delta - \Gamma_o + (z^2/2\sigma^2)] \quad (15)$$

$$\kappa(z)/\kappa'(z) = K_b K_\alpha(z)/K_a = \exp[\Gamma_\infty - (z^2/2\sigma^2)] \quad (16)$$

$$\lambda(z)/\lambda'(z) = K_a/K_b K_\beta(z) = \exp[\Delta - \Gamma_\infty + (z^2/2\sigma^2)] \quad (17)$$

$$\alpha\beta/\alpha'\beta' = \kappa\lambda/\kappa'\lambda' = K_\alpha/K_\beta = e^\Delta \quad (\text{any } z) \quad (18)$$

$$\Gamma_o = \Gamma_\infty - \ln(K_b/K_a) \quad (19)$$

$$z_o^2 = 2\sigma^2\Gamma_o, \quad z_\infty^2 = 2\sigma^2\Gamma_\infty. \quad (20)$$

In the isometric steady state each z value is independent, for computational purposes. This feature is what makes the steady isometric case relatively tractable.
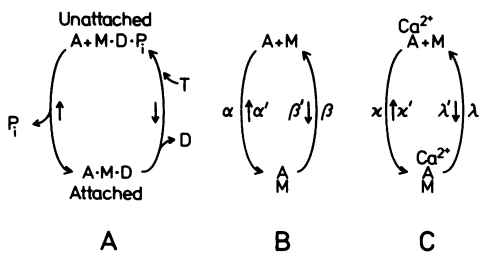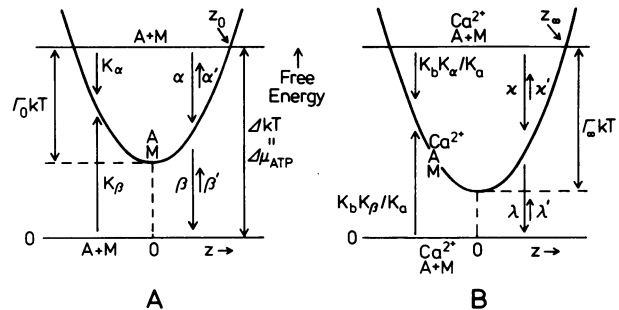

FIGURE 7 (A) Two-state ATPase cycle, with attachment-detachment. D = ADP. Rate constant notation for the cycle without (B) and with (C) Ca^{2+}.

FIGURE 8 Free energy curves corresponding to Fig 7, A and B.

Quasi Equilibrium

If we now make several quite reasonable kinetic assumptions, the formal equations of the equilibrium treatment in the previous section can also be used at steady state. This is possible because of our employment of two-state cycles (27, 28). Cycles with three or more states do not have this quasi-equilibrium property: the analysis becomes much more complicated.

Nearest-neighbor interactions (Fig. 1 B) will perturb the rate constants in Fig. 7 B and C. If we divide the perturbation free energy symmetrically between forward and backward transitions in all four cases, which is plausible because of the complexity of the condensed transitions in Fig. 7 A (6, 13), this is expressed formally by taking the kinetic parameters (27) $f_\alpha = f_\beta = f_\kappa = f_\lambda = \frac{1}{2}$.

The interaction parameters Y_0, Y_∞, and Y_1 arise as in the equilibrium problem. The values depend on the relative compatibility or incompatibility of pairs of Tm ends in states 0, 1, 2 of Fig. 4. State 2 in Fig. 4 refers here specifically to A · M · D (Fig. 7A). Hence it is appropriate to use Y values found for S-1 · ADP (14, 16, 19).

The rate constants in Fig. 7 C are also perturbations of those in Fig. 7 B, owing to the presence of Ca^{2+}. The free energy effects are expressed by (see Eqs. 14–17)

$$\kappa/\kappa' = (\alpha/\alpha')(K_b/K_a)$$
$$\lambda/\lambda' = (\beta/\beta')(K_a/K_b). \tag{21}$$

Physically, the presence of Ca^{2+} reduces the work M has to do against Tm in the attachment process (Fig. 4). The total effect should therefore appear in the rate constant for attachment. Formally, $f_\alpha^{Ca} = 1$ and $f_\beta^{Ca} = 0$ (27), or

$$\kappa = \alpha(K_b/K_a), \qquad \kappa' = \alpha'$$
$$\lambda = \beta, \qquad \lambda' = \beta'(K_b/K_a) \tag{22}$$

for the separate rate constants.

We omit the details (27, 28) but it is easy to show that, with the relations

$$f_\alpha + f_\beta = 1, \qquad f_\kappa + f_\lambda = 1, \qquad f_\alpha^{Ca} + f_\beta^{Ca} = 1 \tag{23}$$

all satisfied, as above, the steady-state distribution of states in Fig. 1 B, including interactions, will have an equilibrium form. To be more specific, in Fig. 3 and in Eqs. 1–11, we merely replace K by

$$s_o(z) = [\alpha(z) + \beta'(z)]/[\beta(z) + \alpha'(z)]. \tag{24}$$

No other parameter changes are needed. If, in Fig. 7 B, the α, α' transitions corresponded to the true equilibrium constant K (i.e., if the β, β' transitions did not occur), then we would have $K = \alpha(\text{on})/\alpha'(\text{off})$. With the β, β' transitions included, the steady-state quasi-equilibrium analogue is $s_o(z)$ = total on/total off = $(\alpha + \beta')/(\beta + \alpha')$ as in Eq. 24. The analogue of the attachment constant $(K_b/K_a)K$, in

Eqs. 4, 11, and elsewhere, is (using Eqs. 22)

$$s_\infty(z) = (\kappa + \lambda')/(\lambda + \kappa')$$
$$= (K_b/K_a)(\alpha + \beta')/(\beta + \alpha') = (K_b/K_a)s_o(z). \tag{25}$$

Thus K_b/K_a automatically plays the same role in the steady-state system as in the equilibrium system. As a consequence of these close analogies with the equilibrium attachment problem, many results of the previous section carry over to the present section.

Attachment at Steady State and at Equilibrium

In the equilibrium attachment of M in Fig. 3, the attachment constant K, with no Ca^{2+} bound, is increased to $(K_b/K_a)K$ when Ca^{2+} is bound. Consequently, the degree of attachment of M to A is increased by Ca^{2+}. At steady state (neglecting here, for simplicity, the reverse or primed rate constants as we do below in section 3), the quantities that determine the degree of attachment, i.e., the analogues of K and $(K_b/K_a)K$ at equilibrium, are rate constant ratios: $\alpha/\beta \simeq s_o$, with no Ca^{2+} bound, and $\kappa/\lambda \simeq s_\infty$ when Ca^{2+} is bound. The detachment steps, β and λ (Figs. 7 and 8), are not the inverses of the attachment steps, α and κ. Furthermore, several successive elementary steps are telescoped into both "attachment" and "detachment" in the simple two-state cycle (Fig. 7 A) we are using. Thus, at steady state, the regulation of the degree of attachment of M · D to A (Fig. 7 A) by Ca^{2+} is not a consequence of the effect of Ca^{2+} on the simple equilibrium binding to M · D to A (as in section 1) but rather of the effect of Ca^{2+} on the attachment and detachment rate constants α and β. According to Eq. 22, in our simple model the presence of Ca^{2+} does not affect β (i.e., $\lambda = \beta$) but α is increased by the factor K_b/K_a [i.e., $\kappa = \alpha(K_b/K_a)$]. The rate constant α and the equilibrium constant K_α refer to the overall process: attachment of M · D · P_i to actin plus P_i release. The free energy decrease in this process, $kT \ln K_\alpha$ (Eq. 12 and Fig. 8 A), is increased in magnitude by Ca^{2+} to $kT \ln(K_b K_\alpha/K_a)$ (Eq. 13 and Fig. 8 B). K_a refers here to binding of Ca^{2+} on Tn with M · D · P_i (Fig. 7 A) unattached, whereas K_b refers to binding of Ca^{2+} on Tn with M · D attached to A (Fig. 4). In the present steady-state model we need Ca^{2+} to be bound more strongly to Tn when M · D is attached to A ($K_b > K_a$). This has a kinetic effect at steady state, converting α to $\kappa = \alpha(K_b/K_a)$ (Eq. 22).

In the simple two-state cycle being used here, α and κ refer to attachment of M · D · P_i to actin plus P_i release. Recent experimental work (23) shows that P_i release is the Ca^{2+}-sensitive part of this over-all process. A more detailed cycle would separate attachment from P_i release.

Isometric Force and ATP Flux

We first discuss the limiting cases $\rho = 0$ (no Ca^{2+}) and $\rho = \infty$ (Ca^{2+} saturation), because they are simpler. The

attachment probability $\theta(z)$ can be calculated from Eq. 9 or 11 using $s_0(z)$ in place of K in Eq. 9 and $s_\infty(z)$ in place of $(K_b/K_a)K$ in Eq. 11. This has to be done at each z. The mean isometric force $\bar{F}$ per cross-bridge is then found by averaging the force $(kT/\sigma^2)z$ of a cross-bridge attached at z over the repeat distance $d = 385$ Å (9, 11, 12):

$$\frac{\bar{F}d}{kT} = \frac{1}{\sigma^2}\int_{-d/2}^{+d/2} \theta(z)\, z\mathrm{d}z. \qquad (26)$$

The mean ATP flux per cross-bridge, $\bar{J}$, is a little more complicated. The values of the perturbed rate constants in the cycle of a given unit, at any particular time, depend on the instantaneous states of the two neighboring units. Thus, it is necessary to count the numbers of triplets of various kinds in the steady state (quasi equilibrium). This has been done elsewhere (26). The result for the flux for a cross-bridge at z, when $\rho = 0$, is (reference 26, Eq. 21)

$$J(z) = \left(\frac{\alpha\beta - \alpha'\beta'}{\beta + \alpha'}\right) \times$$

$$\frac{[(1 - s_0)^2 + 4Y_0^{-1/2}s_0 + (1 + s_0)R_0]\,Y_0^{-1/2}}{R_0[1 + 2Y_0^{-1}s_0 + s_0^2 + (1 + s_0)R_0]}. \qquad (27)$$

Again, as with $\theta(z)$ above, $J(z)$ must be calculated at each z. For the case $\rho = \infty$, substitute everywhere κ for α, λ for β, and subscript ∞ for subscript 0. The effect of these substitutions on the leading parentheses () in Eq. 27 is to multiply by K_b/K_a. Then, in either case, the mean flux is

$$\bar{J} = \frac{1}{d}\int_{-d/2}^{+d/2} J(z)\,\mathrm{d}z. \qquad (28)$$

We turn now to the calculation of $\bar{F}$ and $\bar{J}$ when ρ is arbitrary. Because of the quasi equilibrium, Eqs. 6 and 7 can be used as before (Fig. 6) to find θ (numerically) at arbitrary ρ and z if we replace K by $s_0(z)$ (Eq. 24). No other parameter change is needed. For a given ρ, $\theta(z)$ must be calculated over the range in z. Then, for any ρ, $\bar{F}$ can be obtained using Eq. 26.

The calculation of $J(z)$ at arbitrary ρ and z, to use in Eq. 28, is much more laborious, though the method itself is straightforward. We merely sketch the procedure here. To encompass a triplet in a nearest-neighbor pair of units, we now take two successive Tm molecules as one unit. The units are nonoverlapping. Each unit can be in nine different states (0, 1, 2 × 0, 1, 2), so we must use a 9 × 9 matrix. The x_{ij} interactions occur both within units and between neighboring units. There are 18 kinds of triplets that must be counted. To count a particular type of triplet, say, 000, we introduce a fictitious factor Ψ, for each 000, into each matrix element ij in which the sequence 000 occurs in the pair ij (e.g., the pair 10, 00). Then, in a large array of m Tm molecules, the mean number of 000 triplets is found from

$$\bar{N}_{000} = (m/2)(\Psi\partial\ln\gamma_{max}/\partial\Psi)_{\Psi=1}, \qquad (29)$$

where γ_{max} is the largest eigenvalue of the 9 × 9 matrix. The derivative has to be evaluated numerically. This method is also discussed in reference 29, in relation to its Eq. 30. With the numbers of all triplets available, $J(z)$ can be calculated using the procedure in Eqs. 1–4 of reference 26.

3. NUMERICAL EXAMPLE, MODEL 1

The objective here is to provide a numerical illustration of the above steady state equations. In view of the many simplifications already introduced, we use a very elementary but still significant (12) kinetic model. We first introduce the "physiological" rate constants κ, κ', λ, λ' (i.e., with Ca^{2+} present). The set α, α', β, β' (no Ca^{2+}) then follow from Eqs. 22. Also, with $s_\infty(z)$ specified (Eq. 25), $s_0(z)$ is simply $s_\infty(z)/20$ (taking $K_b/K_a = 20$).

To begin with, we take the parameters of the Ca^{2+} free energy curve to be (13) $\Delta = 23$, $\Gamma_\infty = 20$, and $\sigma^2 = 200$ Å^2. Then $\Gamma_0 = 17.00$. We take κ and λ as constants (12) in the range $z \geq 0$, and $\kappa \simeq 0$, λ finite for $z < 0$. Thus attachment, force generation, and ATPase activity occur only when $z \geq 0$. Specifically, we adopt λ as a reference rate constant (to be evaluated later) and choose $\kappa = 4\lambda$ (to make $s_\infty \simeq 4$, corresponding to $K_bK/K_a = 4$ in Figs. 5 and 6). Then Eqs. 16 and 17 determine the functions $\kappa'(z)/\lambda$ and $\lambda'(z)/\lambda$. These four rate constants are shown in Fig. 9, as functions of z. Also included in the figure is the function

$$s_\infty(z) = [\kappa + \lambda'(z)]/[\lambda + \kappa'(z)]. \qquad (30)$$

Because $\lambda'(z)$ is so small and $\kappa'(z)$ rises so rapidly near $z = 90$ Å, $s_\infty(z)$ has practically a constant value, $s_\infty = 4$, from $z = 0$ to $z = 75$ Å and then drops rather rapidly to zero. The half-value, $s_\infty = 2$, occurs at $z^* = 86.3$ Å.

We should now use $s_0(z)$ and $s_\infty(z)$ from Fig. 9 to calculate $\theta(z)$ and $J(z)$ for insertion in Eqs. 26 and 28. However, as a final simplification and approximation, we adopt the constant values $s_0 = 0.2$, $s_\infty = 4.0$ in the interval $0 \leq z \leq z^*$, and $s_0 = s_\infty = 0$ otherwise. This amounts to neglecting the primed rate constants (back reactions) in this interval, though z^* itself depends on $\kappa'(z)$. Because s_0
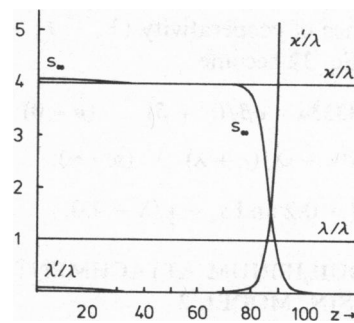

FIGURE 9 Plot of rate constants κ, κ', λ, λ' in an example, as functions of z, all relative to the reference constant λ. Also included is $s_\infty(z)$ from Eq. 30.

and s_∞ are now considered to be constants, θ and J are also constants in the same interval. Also, the leading parentheses in Eq. 27 becomes α in this interval and becomes κ in the $\rho = \infty$ case. Thus we have, from Eqs. 26 and 28,

$$\bar{F}d/kT - \theta z^{*2}/2\sigma^2, \qquad \bar{J} - Jz^*/d. \qquad (31)$$

Isometric Force

Because the values chosen for s_0 and s_∞ are the same as those used for K and $(K_b/K_a)K$, respectively, in Fig. 6, the steady state $\theta(\rho)$ in Eq. 31 is the same as the equilibrium $\theta(\rho)$ in Fig. 6. Hence, the curves in Fig. 6 are also isometric force curves, as indicated by the right-hand ordinate. The conversion factor is $z^{*2}/2\sigma^2 = 18.61$. The limiting values of $\bar{F}d/kT$ for the solid curve are 0.278 at $\rho = 0$ and 17.05 at $\rho = \infty$. As already mentioned, the steepness of the solid curve in Fig. 6 is consistent with in vivo requirements, but it could be made steeper by increasing the cooperativity parameters. Also, experimental force curves (30–34) have this same form. However, the present, illustrative model is too simple to justify the actual fitting of experimental curves.

The experimental value of $\bar{F}d/kT$ at $\rho = \infty$ (taken from reference 13) is 30. As already mentioned, the discrepancy of a factor of ~ 2 is presumably due to the assumption that only a single specific actin site is available for cross-bridge attachment.

Isometric ATP Flux

Because of the complexity mentioned at the end of the previous section, we calculate $\bar{J}$ only for $\rho = 0$ and $\rho = \infty$. Using $s_0 = 0.2$, $Y_0 = 20$ for $\rho = 0$ and $s_\infty = 4.0$, $Y_\infty = 4$ for $\rho = \infty$, Eq. 27 leads to

$$J - 0.2393\alpha - 0.2393 \times 4\lambda/20 \qquad (\rho - 0)$$
$$J - 0.1312\kappa - 0.1312 \times 4\lambda \qquad (\rho - \infty). \qquad (32)$$

Then, with $z^*/d - 0.224$ in Eq. 31, we find $\bar{J} - 0.0107\lambda$ for $\rho - 0$ and $\bar{J} - 0.1176\lambda$ for $\rho - \infty$. The latter flux is larger by a factor of 11. Also, if the experimental value of $\bar{J}(\rho - \infty)$ is taken to be 3 s^{-1} (35), then $\lambda - 25.5$ s^{-1}. The value of κ is then 102 s^{-1}.

In the absence of cooperativity ($Y_0 - Y_\infty - 1$), the two values of J in Eq. 32 become

$$J - 0.8333\alpha - \alpha\beta/(\alpha + \beta) \qquad (\rho - 0)$$
$$J - 0.20\kappa - \kappa\lambda/(\kappa + \lambda) \qquad (\rho - \infty), \qquad (33)$$

using $s_0 - \alpha/\beta - 0.2$ and $s_\infty - \kappa/\lambda - 4.0$.

4. EQUILIBRIUM ATTACHMENT OF MYOSIN, MODEL 2

In Fig. 1 A there are exactly two myosin molecules (M) per Tm unit. The myosin molecules are regularly spaced. The two specific actin sites (x) to which these molecules can attach are designated A and B. The binding of the two M molecules (call them M_A and M_B) to A and B is not equivalent because the position of M_A relative to A is shifted $55/2 = 27.5$ Å compared with the position of M_B relative to B. The details of the model just outlined have been arbitrarily selected for illustrative purposes and ease of calculation; they are almost certainly not realistic.

Fig. 2 shows, for one Tm unit, the four possible states of Tm relative to actin, depending on the binding of Ca^{2+} or of the S-1-N part of a myosin molecule (S-1, subfragment one; N, nucleotide bound to S-1). State 1 (no S-1 bound) is divided into three substates depending on Ca^{2+} binding. Tm is pushed into state 2 when the first M is bound to the unit; binding of Ca^{2+} or of a second M does not alter the position of Tm in state 2 relative to actin (19).

The grand partition function of a single isolated Tm unit is

$$\xi - 1 + 2K_a\rho + \alpha^*K_a^2\rho^2 + \xi_2\xi_b \qquad (34)$$

$$\xi_2 - (K_A + K_B + K_AK_B)/L \qquad (35)$$

$$\xi_b - 1 + 2K_b\rho + \beta^*K_b^2\rho^2. \qquad (36)$$

The terms in Eq. 34 refer to the successive states in Fig. 2. Here ρ is the concentration of Ca^{2+}, K_a is the binding constant of the first Ca^{2+} on a state 1 Tm, α^*K_a is the binding constant of the second Ca^{2+} in state 1, and K_b and β^* are similar for binding Ca^{2+} on a state 2 Tm. Of course α^* and β^* are not to be confused with the rate constants α and β of section 2. The attachment constant of M_A on site A, if M_B is not attached, is K_A/L. If M_B is already attached, this constant is K_A. K_A/L is the analogue of K in section 1, where there is only one M per unit. Similarly, K_B/L and K_B refer to attaching M_B with M_A not attached, or attached, respectively. The factor $L \gg 1$ arises from the work needed (19) to push Tm from its position relative to actin in state 10 to its position in state 2. Thus, for example, it is much easier to attach M_A if M_B is already attached ($K_A \gg K_A/L$). As usual, the separate terms in Eq. 34, including the subterms in Eqs. 35 and 36, are proportional to the corresponding relative populations of the states or substates at equilibrium. This remark applies to isolated Tm units (no cooperativity). We turn now to a long linear array of Tm units, as in Fig. 1 A, where there are nearest-neighbor interactions between Tm units that perturb the equilibrium just described.

There are 10 kinds of nearest-neighbor interactions (19), of which four are illustrated in Fig. 10. We again use the notation $x_{ij} - e^{-w_{ij}/kT}$, where w_{ij} is the ij pair free energy relative to infinite separation of i and j. Like pairs all have the same free energy (19) so that

$$x_{00} - x_{II} - x_{IIII} - x_{22} - x. \qquad (37)$$

In designating pairs, the second subscript (0, I, or II) for state 1 (Fig. 2) is used here and in Fig. 10. Then we define,
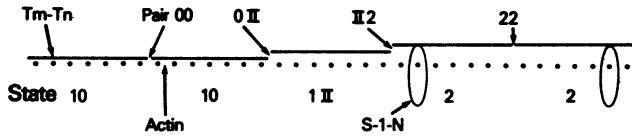
FIGURE 10 Notation used for nearest-neighbor Tm pairs, based on states in Fig. 2. The second subscript (0, I, II) is used for substates of state 1.

for the six unlike pairs,

$$Y_1 = x^2/x_{0I}^2, \quad Y_2 = x^2/x_{0II}^2, \quad Y_0 = x^2/x_{02}^2$$
$$Y_3 = x^2/x_{I II}^2, \quad Y_4 = x^2/x_{I 2}^2, \quad Y_\infty = x^2/x_{II2}^2. \tag{38}$$

This a generalization of the system used in section 1. In the limit $\rho \rightarrow 0$, Y_0 dominates (states 10 and 2 are populated). In the limit $\rho \rightarrow \infty$, Y_∞ dominates (states 1II, and 2 are populated).

The 4×4 matrix corresponding to Eq. 4 in reference 19 (or to Eq. 6 here) is

$$\begin{pmatrix} 1 & X_1 & X_2 & X_0 \\ AX_1 & A & AX_3 & AX_4 \\ BX_2 & BX_3 & B & BX_\infty \\ CX_0 & CX_4 & CX_\infty & C \end{pmatrix} \tag{39}$$

where

$$X_i = Y_i^{-1/2}, \quad A = 2K_a\rho, \quad B = \alpha^*K_a^2\rho^2, \quad C = \xi_2\xi_b. \tag{40}$$

Various mean equilibrium properties can be found (19) by differentiating the largest eigenvalue γ_{max} of Eq. 39. For example, because each state 2 element in Eq. 39 (fourth row) contains a factor C,

$$p_2 = \partial\ln\gamma_{max}/\partial\ln C, \tag{41}$$

where p_2 is the fraction of Tm units in state 2. Within state 2, from Eq. 35, the relative populations of the three kinds of attachment of the two M molecules are proportional to K_A (M_A only), K_B, and $K_A K_B$ (both M's). Thus the probability that A is attached, for a unit in state 2, is

$$\theta_A = (K_A + K_A K_B)/(K_A + K_B + K_A K_B). \tag{42}$$

This is independent of ρ and of cooperativity parameters because of our assumptions about state 2 (19). The over-all fraction of M_A attached is then $p_2\theta_A$. The corresponding fraction for M_B is $p_2\theta_B$.

Limits of High and Low Ca²⁺ Concentration

In the limit $\rho \rightarrow 0$, only states 10 and 2 are significant, and $\xi_b = 1$. Thus Eq. 39 becomes

$$\begin{pmatrix} 1 & X_0 \\ \xi_2 X_0 & \xi_2 \end{pmatrix} \tag{43}$$

Similarly, in the limit $\rho \rightarrow \infty$, only states 1II, and 2 are important, and $\xi_b = \beta^*K_b^2\rho^2$. In this case, after dividing each element by $\alpha^*K_a^2\rho^2$, Eq. 39 reduces to,

$$\begin{pmatrix} 1 & X_\infty \\ \xi_2(\infty)X_\infty & \xi_2(\infty) \end{pmatrix} \tag{44}$$

where

$$\xi_2(\infty) = (K_A + K_B + K_A K_B)/L(\infty) \tag{45}$$

$$L(\infty) = L(\alpha^*K_a^2/\beta^*K_b^2). \tag{46}$$

Eqs. 43 and 44 are alike except that X_∞ replaces X_0 and $L(\infty)$ replaces L. Also, Eq. 43 corresponds to Eq. 8, with ξ_2 in place of K, and Eq. 44 corresponds to Eq. 10, with $\xi_2(\infty)$ in place of $(K_b/K_a)K$. Thus, the analogue here of the important parameter K_b/K_a in section 1 is

$$\xi_2(\infty)/\xi_2 = L/L(\infty) = \beta^*K_b^2/\alpha^*K_a^2. \tag{47}$$

This ratio is almost 20 (1, 19) when M is S-1 (details below). That is, Ca²⁺ binds more strongly on troponin when S-1 is bound to actin. Because, by assumption, $L(\infty) \geq 1$ (i.e., M pushes Tm further than two Ca²⁺ do; see Fig. 2), we must also have $L \geq \beta^*K_b^2/\alpha^*K_a^2$.

When $\rho \rightarrow 0$ or $\rho \rightarrow \infty$, p_2 can be calculated just as in Eqs. 9 and 11 (with the parameter changes mentioned following Eq. 46). Because $\xi_2(\infty) \gg \xi_2$, the population of state 2, p_2, can be much larger at $\rho = \infty$ than at $\rho = 0$ (just as in Fig. 5). The same is then true of the amount of attachment of M_A and M_B because the fraction of M_A attached is $p_2\theta_A$ and the fraction of M_B attached is $p_2\theta_B$. The quantities θ_A and θ_B are independent of ρ and hence have the same values at $\rho = 0$ and $\rho = \infty$.

5. THE STEADY STATE (ISOMETRIC) SYSTEM, MODEL 2

The general principles here are the same as in the discussion of steady states in section 2. However, we have to contend now with more complexity, because there are two M molecules and two Ca²⁺ per unit.

The basic ATPase cycle is, again, that shown in Fig. 7 A. The rate constants, attachment equilibrium constants, and attached-state free energy curves, associated with this cycle under various conditions (see below), are all functions of z. According to our arbitrarily selected model in Fig. 1 A, corresponding free energy curves for A + M_A and B + M_B will be related to each other as shown in Fig. 11. A and B are equivalent sites and M_A and M_B are considered to be equivalent cross-bridges (though they probably come from different thick filaments). Hence the two curves in Fig. 11 are the same except for a lateral shift. As an example, the two points included in Fig. 11 correspond to the particular position of the Tm array relative to the M array pictured in Fig. 1 A in which B is optimally placed for M_B attachment.
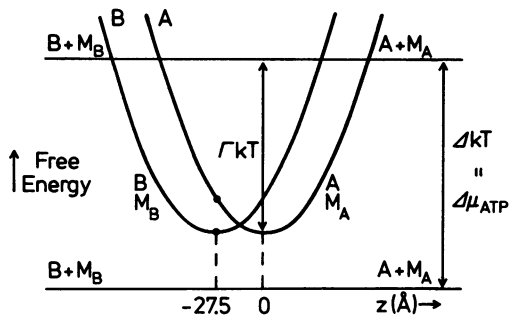
FIGURE 11 Relationship between free energy curves of A + M_A and B + M_B in the section 5 model (Fig. 1 A). $\Delta\mu_{ATP}$ is the free energy of hydrolysis of ATP.

The value of z is arbitrarily defined by the relation of A to M_A, with $z = 0$ set at the free energy minimum for AM_A.

Corresponding to Fig. 7 B, and C, an isolated Tm unit has three kinetic diagrams, depending on the number of Ca^{2+} bound to troponin, as shown in Fig. 12. All transitions are reversible, but the inverse arrows and rate constants (primed, e.g., α'_A is the inverse of α_A) are omitted to simplify the figure. The equilibrium analogue (previous section) of Fig. 12 is presented in Fig. 13, with attachment equilibrium constants included. The state shown in the upper left-hand corner of each diagram in Figs. 12 and 13 belongs to state 1; the other three states in each diagram belong to state 2. Note that the rate constants and attachment constants within state 2 in these figures are independent of the Ca^{2+} state (see Fig. 2).

There are two attachment equilibrium constants for each cycle, related to rate constants (all of these "constants" are functions of z):

$$\alpha_A/\alpha'_A = K_{A\alpha}/L, \qquad \beta'_A/\beta_A = K_{A\beta}/L \tag{48}$$

$$\mu_A/\mu'_A = (K_{A\alpha}/L)(K_b/K_a), \qquad \nu'_A/\nu_A = (K_{A\beta}/L)(K_b/K_a) \tag{49}$$

$$\kappa_A/\kappa'_A = (K_{A\alpha}/L)(\beta^*K_b^2/\alpha^*K_a^2),$$

$$\lambda'_A/\lambda_A = (K_{A\beta}/L)(\beta^*K_b^2/\alpha^*K_a^2) \tag{50}$$

$$a_A/a'_A = K_{A\alpha}, \qquad b'_A/b_A = K_{A\beta}. \tag{51}$$

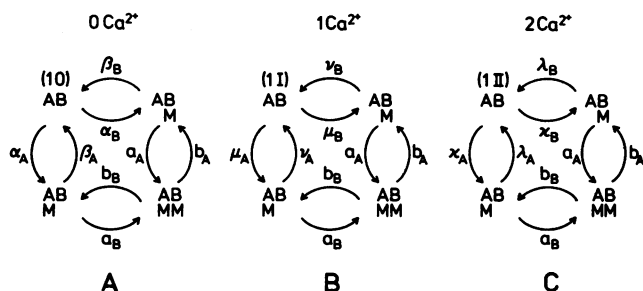Another set of equations follows on replacing subscript A

FIGURE 12 Rate constant notation used for the kinetic diagram of one isolated Tm unit, depending on the number of Ca^{2+} bound to troponin. A and B are actin sites, M is a myosin molecule (one S-1 head attached).
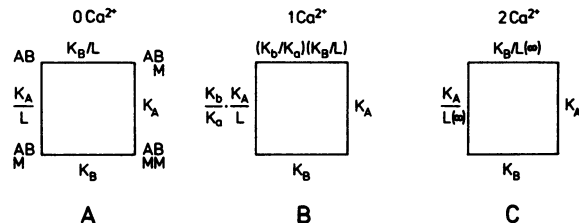

FIGURE 13 Equilibrium version of Fig. 12, showing attachment equilibrium constants rather than rate constants.

by B. All of these cycles satisfy the same thermodynamic force relation, e.g.,

$$a_A b_A/a'_A b'_A = K_{A\alpha}/K_{A\beta} = e^\Delta \qquad \text{(any } z) \tag{52}$$

$$a_B b_B/a'_B b'_B = K_{B\alpha}/K_{B\beta} = e^\Delta \qquad \text{(any } z)$$

where $\Delta \equiv \Delta\mu_{ATP}/kT$.

The deepest free energy well for an attached state (see ΓkT in Fig. 11) occurs in the a, b cycles, because the strongest attachment of M, with constant $K_{A\alpha}$ or $K_{B\beta}$, occurs when another M is already attached. The depth of the a_A, b_A well is the same as that of the a_B, b_B well (Fig. 11). The free energy minimum in the κ,λ cycles (two Ca^{2+} bound) is higher than in a,b by $kT \ln L(\infty)$; the free energy minimum in the μ, ν cycles is higher than in a,b by $kT \ln(LK_a/K_b)$; and the minimum in the α, β cycles is higher than in a, b by $kT \ln L$. Thus we have a whole family of free energy curves to relate to rate constants (as in Fig. 8 and Eqs. 14–17).

Quasi Equilibrium

We make the same plausible assumptions here about kinetic parameters as in section 2. As a consequence, individual rate constant relations are

$$\mu_A = \alpha_A(K_b/K_a), \qquad \mu'_A = \alpha'_A$$
$$\nu'_A = \beta'_A(K_b/K_a), \qquad \nu_A = \beta_A \tag{53}$$

$$\kappa_A = \alpha_A(\beta^*K_b^2/\alpha^*K_a^2), \qquad \kappa'_A = \alpha'_A$$
$$\lambda'_A = \beta'_A(\beta^*K_b^2/\alpha^*K_a^2), \qquad \lambda_A = \beta_A \tag{54}$$

$$a_A = \alpha_A L, \qquad a'_A = \alpha'_A$$
$$b'_A = \beta'_A L, \qquad b_A = \beta_A. \tag{55}$$

Another set follows on replacing subscript A by B. Incidentally, this particular assignment (Eqs. 53–55) is not essential so long as relations like Eqs. 23 are satisfied. We find from Eqs. 53–55,

$$[(\alpha_A + \beta'_A)/(\beta + \alpha'_A)] = [(a_A + b'_A)/(b_A + a'_A)]/L \tag{56}$$

$$[(\mu_A + \nu'_A)/(\nu_A + \mu'_A)]$$
$$= [(a_A + b'_A)/(b_A + a'_A)](K_b/K_a L) \tag{57}$$

$$[(\kappa_A + \lambda'_A)/(\lambda_A + \kappa'_A)] = [(a_A + b'_A)/(b_A + a'_A)]/L(\infty). \tag{58}$$

There are corresponding equations with subscript A replaced by B. In this quasi-equilibrium steady state there is "detailed balance" as at equilibrium. Fig. 12 can be treated formally like Fig. 13. The bracket [] on the right-hand side of Eqs. 56–58 is the steady state analogue of K_A in Fig. 13. The three brackets on the left-hand side of Eqs. 56–58 are the analogues, respectively, of K_A/L in Fig. 13 A, of $(K_b/K_a)(K_A/L)$ in Fig. 13 B, and of $K_A/L(\infty)$ in Fig. 13 C. The brackets are all functions of z; the above comments apply at any z. In fact, the four brackets mentioned all have the same z dependence; they differ only by constant factors. All of the B rate constants and brackets have the same z dependence as their A analogues, except for a shift of 27.5 Å (Fig. 11).

The perturbations of rate constants owing to nearest-neighbor interactions can also be treated in a quasi-equilibrium fashion (26) if we assume $f_\alpha = f_\beta = \frac{1}{2}$, etc., as in section 2.

Thus, the calculation of state probabilities in this quasi-equilibrium steady-state, including the effects of neighbor interactions, is carried out just as in the previous section for the equilibrium case. All that is required is a change in parameters. We define

$$r_A(z) = (a_A + b_A')/(b_A + a_A') \tag{59}$$

$$r_B(z) = (a_B + b_B')/(b_B + a_B') \tag{60}$$

$$u_0(z) = (r_A + r_B + r_A r_B)/L. \tag{61}$$

Hence r_A, r_B, and u_0 correspond to K_A, K_B, and ξ_2 at equilibrium (Eq. 35). In using Eqs. 39 and 40 at arbitrary ρ, for a steady state, the only change necessary is to replace ξ_2 in Eqs. 40 by $u_0(z)$. Eq. 41 is still used to find $p_2(z)$ and Eq. 42 becomes

$$\theta_A(z) = (r_A + r_A r_B)/(r_A + r_B + r_A r_B), \tag{62}$$

with a similar expression for $\theta_B(z)$.

In the limit $\rho \to 0$, Eq. 43 is the pertinent matrix with ξ_2 replaced by $u_0(z)$. Eq. 9 can be used to calculate $p_2(z)$, if we replace K by $u_0(z)$. In the limit $\rho \to \infty$, the matrix Eq. 44 applies, with $u_\infty(z)$ in place of $\xi_2(\infty)$, where

$$u_\infty(z) = (r_A + r_B + r_A r_B)/L(\infty) = u_0(z)L/L(\infty). \tag{63}$$

Note that the functions $u_\infty(z)$ and $u_0(z)$ differ only by a constant factor. Eq. 11 then gives $p_2(z)$ if $(K_b/K_a)K$ is replaced by $u_\infty(z)$. It is clear from the above comments that $u_0(z)$ is an effective steady state "equilibrium constant" for formation of state 2 from state 1, when $\rho \to 0$, and $u_\infty(z)$ has the same significance for $\rho \to \infty$. State 2 includes three substates (only M_A attached, only M_B attached, both attached), which have their own internal quasi-equilibrium distribution (see, e.g., Eq. 62).

Isometric Force

At steady state, for an arbitrary z value (Fig. 11), the fraction of M_A attached is $p_2(z)\theta_A(z)$ and the fraction of

M_B attached is $p_2(z)\theta_B(z)$. The force exerted on actin by an attached A is $(kT/\sigma^2)z$, where kT/σ^2 is the force constant. Similarly, for an attached B, the force is $(kT/\sigma^2)(z + 27.5)$. thus the mean force $\bar{F}$ per cross-bridge is given by

$$\frac{\bar{F}d}{kT} = \frac{1}{2\sigma^2} \int_{-d/2}^{+d/2} [p_2(z)\theta_A(z)z + p_2(z)\theta_B(z)(z + 27.5)] \, dz, \tag{64}$$

where $d = 385$ Å is the actin repeat distance and the factor of 2 averages between M_A and M_B.

Isometric ATP Flux

The ATP flux can be calculated as shown schematically in Fig. 14 A. At any z, the total ATP flux per Tm unit, $J(z)$, has four contributions, $J_1, \ldots, J_4$. Each of these is the net transition flux (11) for the transition indicated by an arrow. Substates with different Ca^{2+} binding are not shown here explicitly.

J_1 and J_2 can be combined, as in Fig. 14 B. This is flux associated with "first M" attachment. Because the interactions with neighbor units change in any change of state $1 \to 2$ or $2 \to 1$, $J_1 + J_2$ can be evaluated only if the mean numbers of all triplets of Tm units are available (26). At an arbitrary ρ, there are 40 types of triplets whose populations can be found numerically from a 16×16 matrix (Eq. 29). In the special cases $\rho \to 0$ and $\rho \to \infty$, this complexity is much reduced and the triplet numbers are already available analytically (26).

The calculation of J_3 and J_4 (Fig. 14 A) is easy because the interactions of the given unit with its neighbors do not change in these transitions (interactions do not depend on the substates of state 2). These transitions refer to attachment-detachment of M ("second M") when the other M is already attached. We define

$$p_A(z) \equiv r_A/(r_A + r_B + r_A r_B), \tag{65}$$

and similarly for $p_B(z)$. Eq. 65 gives the probability a unit that is in state 2 has M_A attached but not M_B. Then

$$J_3(z) = p_2 p_A a_B - p_2(1 - p_A - p_B)a_B'$$
$$J_4(z) = p_2 p_B a_A - p_2(1 - p_A - p_B)a_A'. \tag{66}$$

The mean ATP flux per cross-bridge is

$$\bar{J} = \frac{1}{2d} \int_{-d/2}^{+d/2} [J_1(z) + \cdots + J_4(z)] \, dz. \tag{67}$$
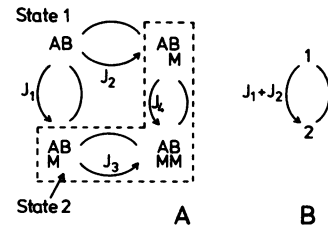

FIGURE 14 (*A*) Four contributions to ATP flux. (*B*) Composite flux $J_1 + J_2$, in the two-state cycle.

ATP Flux at $\rho \rightarrow 0$ and $\rho \rightarrow \infty$

We can be explicit about $J_1 + J_2$ in these special cases. When $\rho \rightarrow 0$, only states 10 and 2 are important (Fig. 1 A). The rate constants in the simulated two-state cycle, Fig. 14 B, can be deduced from Figs. 12 A, 14 A and Eq. 65. Corresponding to Eq. 27, we then find (26)

$$J_1(z) + J_2(z)$$
$$= () \frac{[(1 - u_0)^2 + 4Y_0^{-1/2}u_0 + (1 + u_0)R_0]Y_0^{-1/2}}{R_0[1 + 2Y_0^{-1}u_0 + u_0^2 + (1 + u_0)R_0]}, \quad (68)$$

where

$$R_0 = [(1 - u_0^2 + 4u_0 Y_0^{-1}]^{1/2} \quad (69)$$

$$() = \frac{(\alpha_A + \alpha_B)(\beta_A p_A + \beta_B p_B) - (\alpha'_A p_A + \alpha'_B p_B)(\beta'_A + \beta'_B)}{\beta_A p_A + \beta_B p_B + \alpha'_A p_A + \alpha'_B p_B}. \quad (70)$$

Note that Eq. 70 simplifies to $() = \alpha_A + \alpha_B$ if the inverse (primed) transitions are neglected. In the limit $\rho \rightarrow \infty$ (states 1II, and 2), Eqs. 68–70 still apply if we substitute subscript ∞ for 0, κ for α, and λ for β (Fig. 12). From Eqs. 54 we see that the effect of these substitutions on the leading $()$ in Eq. 68 is to multiply by the factor $\beta^* K_b^2 / \alpha^* K_a^2$, or $L/L(\infty)$.

6. NUMERICAL EXAMPLE, MODEL 2

The example we use here is very similar to that in section 3. In fact, we adjust parameters to make it as similar as possible.

The "physiological" rate constants are considered to be the a,b set (attachment-detachment with one M already attached). These rate constants come into play only in state 2, which is significantly occupied only at high enough Ca^{2+} (bound Ca^{2+} enhances the attachment of the first attached M). Any rate constant function for M_A, say $a_A(z)$, is related to the same function for M_B by $a_A(z) = a_B(z - 27.5)$.

We take $L = 50$ and $\beta^* K_b^2 / \alpha^* K_a^2 = 20$. These are rounded off slightly from values found in reference 19. Then $L(\infty) = 2.5$. The individual Ca^{2+} parameters adopted (compare reference 19) to give the factor 20, above, are $K_a = 3.6 \times 10^6 \, M^{-1}$, $K_b = 10^7 \, M^{-1}$, $\alpha^* = 0.1543$, and $\beta^* = 0.40$. Eqs. 53–55 then relate the other rate constant sets to the a,b set.

As in section 3, we take the functions $a_A(z)$ and $b_A(z)$ to be constants for $z \geq 0$, and $a_A(z) \approx 0$ for $z < 0$. Thus all the "action" for M_A takes place at positive z. We use b_A as a reference constant, to be evaluated later, and take $a_A/b_A = 2.317$. This particular value is chosen so that we will have $u_\infty = 4$ (Eq. 63) in the principal z interval (see below). In section 3, we used, correspondingly, $s_\infty = 4$. As in section 3, we have (see Eqs. 51)

$$a_A/a'_A = K_{A\alpha} = \exp[\Gamma - (z^2/2\sigma^2)] \quad (71)$$

$$b_A/b'_A = 1/K_{A\beta} = \exp[\Delta - \Gamma + (z^2/2\sigma^2)] \quad (72)$$

for the relations between rate constants and free energies. For the corresponding B functions, replace z by $z + 27.5$ Å. These equations then give $b'_A(z)/b_A$ and $a'_A(z)/b_A$. On substituting into Eq. 59, we obtain $r_A(z)$. The function $r_A(z)$ is practically constant at the value 2.317 from $z = 0$ until the neighborhood of $z = (2\sigma^2 T)^{1/2}$, where r_A drops rather quickly to zero (just as s_∞ does in Fig. 9). Using $\Delta = 23$, and $\sigma^2 = 200 \, Å^2$, as before, $r_A(z)$ falls to its half-value (1.158) at $z = 86.3$ Å (as in section 3) if we choose $\Gamma = 19.455$ (instead of $\Gamma_\infty = 20$, as in section 3).

We now approximate $r_A(z)$ by the step function shown by the solid lines in Fig. 15 ($r_A = 2.317$ in the interval $0 \leq z \leq 86.3$ Å). The function $r_B(z)$ has the same shape but is shifted 27.5 Å to the left. Then $u_\infty(z)$ follows from Eq. 63 and is shown by the dotted lines (three branches) in Fig. 15. In the interval $0 \leq z \leq 58.8$ Å, u_∞ has the value 4 (as mentioned above). In this interval of the z axis, both M_A and M_B can attach; $u_\infty = 4$ is the effective state 1 $\rightarrow$ state 2 "equilibrium constant" when this is the case. In the interval -27.5 Å $\leq z \leq 0$ only M_B can attach; in the interval 58.8 Å $\leq z \leq 86.3$ Å only M_A can attach. In the latter two intervals, $u_\infty = 2.317/2.5 = 0.93$. Recall that (Eq. 53) $u_0(z) = u_\infty(z)/20$. Thus $u_0 = 0.2$ in the main central interval.

With $r_A(z)$ and $r_B(z)$ specified (Fig. 15), the functions $\theta_A(z)$ and $\theta_B(z)$ follow from Eq. 62. It will be recalled that $\theta_A(z)$, for example, is the probability that M_A is attached for a unit in state 2. This function steps down (Fig. 15) from $\theta_A = 1$, to $\theta_A = 0.768$, to $\theta_A = 0$, and similarly for θ_B, in the reverse direction.

As already pointed out, with our choices of a_A and b_A the use of a "box" function for r_A in Fig. 15 is equivalent to assuming a one-way cycle (neglect primed rate constants), except that $a'_A(z)$ is involved in fixing the cutoff point (86.3 Å).

Isometric Force

At any ρ, the integral in Eq. 64 is carried out over the range of z shown in Fig. 15. The factors in the integrand of Eq. 64 are all constant within the three subranges of Fig. 15,
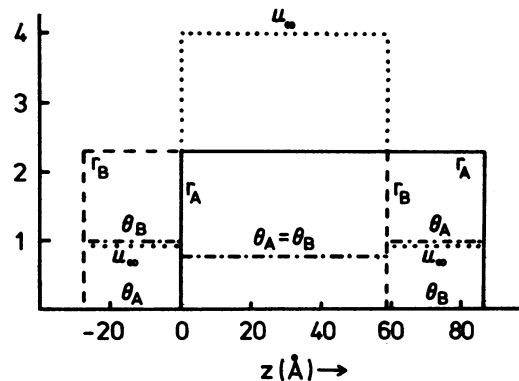

FIGURE 15   Functions chosen from $r_A(z)$ and $r_B(z)$ in numerical example. The functions u_∞, θ_A and θ_B then follow; also, $u_0 = u_\infty/20$.

except z and $z + 27.5$. Hence the integrals are very simple (see Eq. 31). The values of θ_A and θ_B have been discussed already (Fig. 15), and are independent of ρ. The values of $p_2(\rho)$ in the three subranges (only two are different) are found from the u_0 values (i.e., from $u_\infty/20$ in Fig. 15) and Eq. 41 (u_0 replaces ξ_2 in Eq. 40). However, before using Eq. 41, the cooperativity parameters Y_i in Eq. 38 must be specified. To begin with, we take $Y_0 = 20$ and $Y_\infty = 4$, as in section 3. Larger values of Y_0 and Y_∞ would produce steeper curves, below. Using the argument mentioned in section 1, we might then guess $Y_1 = \sqrt{5}$, $Y_2 = 5$, $Y_3 = \sqrt{5}$, and $Y_4 = 4\sqrt{5}$, if $Y_2 = 5$ (from $Y_0/Y_\infty = 5$) is evenly split in the two Ca^{2+} binding steps. This is a plausible set of Y_i values, but still quite arbitrary. We call this the "symmetrical" case.

For use in Eq. 64, the calculated upper dashed curve in Fig. 16 gives $p_2\theta_A$ or $p_2\theta_B$, as a function of ρ, in the main interval II (inset, Fig. 16). This is the probability that A is attached (or that B is attached) for any z in this interval. The two limiting values of p_2 are 0.015 ($\rho \to 0$) and 0.916 ($\rho \to \infty$), just as for θ in section 1. The lower dashed curve in Fig. 16 gives p_2 as a function of ρ in interval I ($\theta_B = 1$, $\theta_A = 0$) or in interval III ($\theta_A = 1$, $\theta_B = 0$). This is the probability that M is attached when only one M can attach. The calculated force per myosin molecule is then found (Eq. 64) as the dashed line in Fig. 17. This curve is moderately steep; experimental curves are steeper (30–34).

For comparison, the dotted curves in Figs. 16 and 17 follow from the corresponding noncooperative case: all $Y_i = 1$.

As an alternative (there are many possibilities), still using $Y_0 = 20$, $Y_\infty = 4$, and $Y_2 = Y_0/Y_\infty = 5$, we take $Y_1 = 1$, $Y_3 = 5$, $Y_4 = 20$ (the "unsymmetrical" case). This assumes that the first bound Ca^{2+} does not move Tm at all, but the second one does. This choice of the Y_i leads to the solid curves in Figs. 16 and 17. The limits at $\rho \to 0$ and $\rho \to \infty$ are unchanged. The cooperativity exhibited in these curves is stronger. Use of larger Y_i values would produce still steeper curves, but we do not pursue this point systematically because the model is too arbitrary. Qualitatively, though, it is clear that this class of model can account for
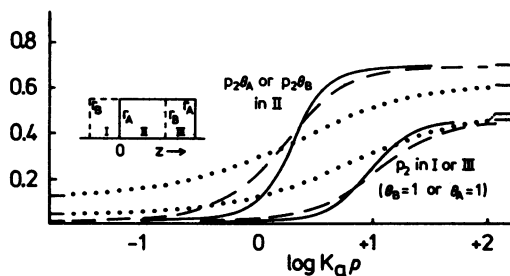

FIGURE 16 Calculated curves, in numerical example, of $p_2\theta_B$ in region I (see inset), of $p_2\theta_A$ or $p_2\theta_B$ in region II, and of $p_2\theta_A$ in region III, for three choices of cooperativity parameters. Inset represents r_A and r_B from Fig. 15. ——, unsymmetrical; – – –, symmetrical; · · ·, no cooperativity.
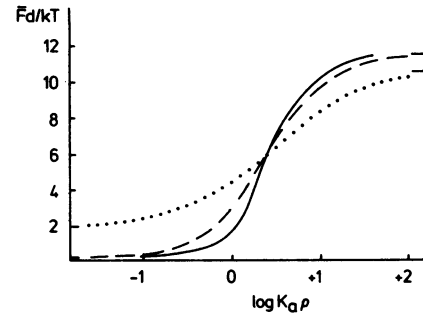

FIGURE 17 Calculated curves of isometric force as a function of Ca^{2+} concentration (ρ). $\bar{F}$ is the force per myosin molecule. ——, unsymmetrical; – – –, symmetrical; · · ·, no cooperativity.

strong cooperativity in the isometric force as a function of Ca^{2+} concentration. The crossing point of the two cooperativity curves in Fig. 17 occurs at pCa = 6.1 (using the value of K_a already given).

Isometric ATP Flux

The calculation of $\bar{J}$ (Eq. 67), at arbitrary ρ, is too tedious (see the preceding section) to be worth carrying out for this model. Incidentally, an exception (which likewise we do not pursue here) is the case $Y_1 = Y_2 = Y_3 = 1$, $Y_0 = Y_4 = Y_\infty > 1$. This corresponds physically to neither bound Ca^{2+} moving Tm, though M does. We still have $L > L(\infty)$ (Ca^{2+} binds more strongly on troponin in state 2). In this case, the equilibrium 4×4 matrix, Eq. 39, is replaced by a 2×2 matrix:

$$\begin{pmatrix} \xi_a & \xi_a X_0 \\ \xi_2\xi_b X_0 & \xi_2\xi_b \end{pmatrix} \tag{73}$$

where $\xi_a = 1 + A + B$ (Eq. 40). Triplet numbers can then be found and used as in reference 26.

We turn now to the limits $\rho \to 0$ and $\rho \to \infty$ ("symmetrical" and "unsymmetrical" cases are the same in these limits). The numerical example we are considering here corresponds to the use of one-way cycles, as mentioned above. Hence, in Eqs. 66 and 70,

$$J_3 = p_2 p_A a_B, \qquad J_4 = p_2 p_B a_A \tag{74}$$

$$() = \alpha_A + \alpha_B = (a_A + a_B)/L \qquad (\rho \to 0) \tag{75}$$

$$= \kappa_A + \kappa_B = (a_A + a_B)/L(\infty). \qquad (\rho \to \infty)$$

$J_1 + J_2$ (first M) must be evaluated in regions I, II, and III (inset, Fig. 16), using Eq. 68 (the calculation in regions I and III is the same). $J_3 + J_4$ (second M) refers to region II only. We find, from the two contributions (Eq. 67),

$$2\bar{J} = \bar{J}_{1+2} + \bar{J}_{3+4} = 0.0021a_A + 0.0011a_A$$
$$= 0.0032a_A \qquad (\rho \to 0) \tag{76}$$

$$2\bar{J} = 0.0423a_A + 0.0648a_A = 0.1071a_A. \qquad (\rho \to \infty) \tag{77}$$

"First M" flux predominates at $\rho \to 0$ and "second M"

flux at $\rho \to \infty$. The experimental value of $\bar{J}$ at $\rho = \infty$ (see section 3) is 3 s^{-1}. On comparison with Eq. 77, we need $a_A = 56$ s^{-1} and $b_A = 24$ s^{-1}. Correspondingly, in section 3 we require $\lambda = 25.5$ s^{-1}. The flux ratio between $\rho \to \infty$ and $\rho \to 0$ is 34 (this ratio was 11 in section 3).

REFERENCES

1. Bremel, R. D., and A. Weber. 1972. Cooperation within actin filaments in vertebrate skeletal muscle. *Nat. New Biol.* 238:97–101.

2. Haselgrove, J. C. 1973. X-ray evidence for the conformational change in the actin-containing filaments of vertebrate striated muscle. *Cold Spring Harbor Symp. Quant. Biol.* 37:341–352.

3. Huxley, H. E. 1973. Structural changes in the actin- and myosin-containing filaments during contraction. *Cold Spring Harbor Symp. Quant. Biol.* 37:361–376.

4. Bremel, R. D., J. M. Murray, and A. Weber. 1973. Manifestations of cooperative behavior in the regulated actin filament during actin-activated ATP hydrolysis in the presence of calcium. *Cold Spring Harbor Symp. Quant. Biol.* 37:267–276.

5. Murray, J. M., and A. Weber. 1974. The cooperative action of muscle proteins. *Sci. Am.* 230:59–71.

6. Adelstein, R. S., and E. Eisenberg. 1980. Regulation and kinetics of the actin-myosin-ATP interaction. *Annu. Rev. Biochem.* 49:921–956.

7. Huxley, A. F. 1957. Muscle structure and theories of contraction: a hypothesis for the mechanism of contraction. *Prog. Biophys. Mol. Biol.* 7:255–318.

8. Hill, T. L. 1968. On the sliding filament model of muscular contraction. *Proc. Natl. Acad. Sci. USA.* 61:98–105.

9. Hill, T. L. 1974. Theoretical formalism for the sliding filament model of contraction of striated muscle, Part I. *Prog. Biophys. Mol. Biol.* 28:267–340.

10. Hill, T. L. 1975. Theoretical formalism for the sliding filament model of contraction of striated muscle, Part II. *Prog. Biophys. Mol. Biol.* 29:105–159.

11. Hill, T. L. 1977. Free Energy Transduction in Biology. Academic Press, Inc., New York. 1–229.

12. Hill, T. L., E. Eisenberg, Y.-D. Chen, and R. J. Podolsky. 1975. Some self-consistent two-state sliding filament models of muscle contraction. *Biophys. J.* 15:335–372.

13. Eisenberg, E., T. L. Hill, and Y.-D. Chen. 1980. Cross-bridge model of muscle contraction. Quantitative analysis. *Biophys. J.* 29:195–227.

14. Greene, L. E., and E. Eisenberg. 1980. Cooperative binding of myosin subfragment-1 to the actin-troponin-tropomyosin complex. *Proc. Natl. Acad. Sci. USA.* 77:2616–2620.

15. Wegner, A. 1979. Equilibrium of the actin-tropomyosin interaction. *J. Mol. Biol.* 131:839–853.

16. Hill, T. L., E. Eisenberg, and L. Greene. 1980. Theoretical models for the cooperative equilibrium binding of myosin subfragment-1 to the actin-troponin-tropomyosin complex. *Proc. Natl. Acad. Sci. USA.* 27:3186–3190.

17. Hill, T. L., E. Eisenberg, and J. M. Chalovich. 1981. Theoretical models for the cooperative steady-state ATPase activity of myosin subfragment-1 on regulated actin. *Biophys. J.* 35:99–112.

18. Hill, T. L. 1981. Binding under a molecular "umbrella" as a cooperative statistical mechanical system: Tropomyosin-actin-myosin as an example. *Biophys. Chem.* 14:31–44.

19. Hill, T. L., E. Eisenberg, and L. Greene. 1983. Alternate model for the cooperative equilibrium binding of myosin subfragment-1-nucleotide complex to actin-troponin-tropomyosin. *Proc. Natl. Acad. Sci. USA.* 80:60–64.

20. Tregear, R. T., and J. M. Squire. 1973. Myosin content and filament structure in smooth and striated muscle. *J. Mol. Biol.* 77:279–290.

21. Squire, J. M. 1973. General model of myosin filament structure. III. *J. Mol. Biol.* 77:291–310.

22. Hill, T. L., and E. Eisenberg. 1979. *In* Cross-Bridge Mechanism in Muscle Contraction. H. Sugi and G. H. Pollack, editors. University of Tokyo, 541–560.

23. Chalovich, J. M., and E. Eisenberg. 1982. Inhibition of actomyosin ATPase activity by troponin-tropomyosin without blocking the binding of myosin to actin. *J. Biol. Chem.* 257:2432–2437.

24. Hill, T. L. 1960. Statistical Thermodynamics. Addison-Wesley, Reading, MA. 1–508.

25. Hill, T. L. 1978. Binding of monovalent and divalent myosin fragments onto sites on actin. *Nature (Lond.).* 274:825–826.

26. Hill, T. L. 1977. Further study of the effect of enzyme-enzyme interactions on steady-state enzyme kinetics. *Proc. Natl. Acad. Sci. USA.* 74:4111–4115.

27. Hill, T. L. 1977. Theoretical study of the effect of enzyme-enzyme interactions on steady-state enzyme kinetics. *Proc. Natl. Acad. Sci. USA.* 74:3632–3636.

28. Hill, T. L. 1978. Effect of enzyme-enzyme interactions on steady-state enzyme kinetics. IV. Strictly steady-state examples. *J. Theor. Biol.* 75:391–416.

29. Hill, T. L. 1982. On the one-dimensional steady-state Ising problem. *J. Chem. Phys.* 76:1122–1127.

30. Hellam, D. C., and R. J. Podolsky. 1969. Force measurements in skinned muscle fibers. *J. Physiol. (Lond.).* 200:807–819.

31. Julian, F. J. 1972. The effect of calcium on the force-velocity relation of briefly glycerinated muscle fibers. *J. Physiol. (Lond.).* 218:117–145.

32. Brandt, P. W., R. N. Cox, and M. Kawai. 1980. Can the binding of Ca^{2+} to two regulatory sites on troponin C determine the steep pCa/tension relationship of skeletal muscle? *Proc. Natl. Acad. Sci. USA.* 77:4717–4720.

33. Brandt, P. W., R. N. Cox, M. Kawai, and T. Robinson. 1982. Regulation of tension in skinned muscle fibers. Effect of cross-bridge kinetics on apparent Ca^{2+} sensitivity. *J. Gen. Physiol.* 79:997–1016.

34. Godt, R. E., and B. D. Lindley. 1982. Influence of temperature upon contractile activation and isometric force production in mechanically skinned muscle fibers of the frog. *J. Gen. Physiol.* 80:279–297.

35. Curtin, N. A., C. Gilbert, K. M. Kretzschmar, and D. R. Wilkie. 1974. The effect of the performance of work on total energy output and metabolism during muscular contraction. *J. Physiol.* (Lond.). 238:455–472.